www.cad-journal.net
Computer-Aided Design AND APPLICATIONS

Topology Optimization Method for Multi-Patch FDM Printing Based on Dynamic Loads and Anisotropic Characteristics

Kaiyuan Meng[1] and Jikai Liu[1*]

[1] Key Laboratory of High Efficiency and Clean Mechanical Manufacture (Ministry of Education), School of Mechanical Engineering, Shandong University, Jinan, China, jikai_liu@sdu.edu.cn

Corresponding author: Jikai Liu, jikai_liu@sdu.edu.cn

Abstract. This paper introduces a topology optimization method specifically designed for multi-patch fused deposition modeling (FDM) printing. The method simultaneously optimizes the structural topology and patch-wise printing directions to improve performance under dynamic loads while taking account of the material anisotropy. Specifically, an enhanced double smoothing projection (DSP) filter is implemented to distinguish between the contour offset layer and the substrate domain. The solid orthotropic material with penalty (SOMP) interpolation method is adopted to capture the density-related material properties. By using the extended-solid isotropic material with penalization (SIMP) method, substrate domains (patches) with varying orientations are distinguished and treated as distinct materials, facilitating the coupled optimization of patch-wise orientations and density distribution. Numerical examples illustrate that this method significantly reduces the dynamic compliance of the structure while increasing its natural frequency. This work provides both a theoretical framework and a practical manufacturing solution for multi-patch FDM printing, contributing to the advancements in dynamic structural design for additive manufacturing (AM).

Keywords: Topology Optimization; Hybrid Deposition Path; Multi-Patch Design; Material Anisotropy
DOI: https://doi.org/10.14733/cadaps.2026.778-789

1 INTRODUCTION

Additive manufacturing (AM) technology, with its manufacturing method of depositing materials layer by layer, can realize the processing of complex geometric shapes, breaking the limitations of traditional manufacturing processes, providing greater freedom for performance-oriented design, and effectively avoiding manufacturability issues [1]. Design for Additive Manufacturing (DfAM) aims at generating geometries that meet manufacturing requirements while maximize performance [2]. As a powerful design method, topology optimization (TO) has gradually become an ideal choice in this field because of fully utilizing the flexibility of DfAM [3]. In recent years,

more and more studies have incorporated the constraints inherent in additive manufacturing into the topology optimization framework, such as limiting the overhang angle and controlling the size scale of design features [4,5]. These innovations have provided new development directions for topology optimization in AM and promoted the application and advancement of this method [6].

Since AM adopts a layer-by-layer manufacturing method, almost all AM materials exhibit varying degrees of anisotropic characteristics [7], and this phenomenon is particularly obvious in fused deposition modeling (FDM). In fact, fully considering the anisotropic properties of materials in topology optimization can effectively narrow the performance gap between the designed structure and the actual manufactured structure.

Taking fiber composite 3D printing as an example, the initial research idea is to use fiber angle as a complementary variable field to achieve collaborative design of structural topology optimization and fiber deposition direction optimization. However, the discrete definition of the angle leads to disordered fiber orientation distribution [8], which makes it extremely difficult to extract effective fiber deposition paths from the optimization results for machine execution. In order to solve this problem, Lee et al. [9] proposed a method to discretize the topology into unidirectionally deposited components to achieve segmented continuous fiber orientation optimization to reduce the complexity of the fiber orientation field. Subsequently, Papapetrou et al. [10] further post-processed the optimized fiber orientation and proposed a variety of fiber deposition modes, including contour offset mode, streamline mode and isometric mode, to improve the implement ability of the deposition path. To address the issues of discretely defining the fiber angles, Ren et al. [11] adopted a wave function to project the fiber reinforcement scale field onto a background mesh, which realized the concurrent optimization of structural topology and equal-space fiber trajectories.

However, the equal-space method does not provide a gap/overlap-free deposition path pattern, making it infeasible for many 3D printing machines. In practical applications, most FDM machines only support the hybrid deposition path (HDP) mode, which achieves material deposition by filling the internal structure after the contour offset in a zigzag shape. Therefore, for this mode, Liu et al. [12] proposed a level set-based method that combines hybrid deposition path planning with shape optimization and topology optimization to improve the performance of the printed structure. In addition, Xu et al. [13] used the SIMP method to carry out topology optimization research based on HDP, fully considering the influence of material anisotropy in the topological design process. Meng et al. [14] further expanded this method to the dynamic level, using dynamic compliance as the optimization goal to study the dynamic response of the structure under various excitation conditions, and verified the effectiveness through numerical calculations and experiments.

It is worth noting that in existing studies on co-optimization of printing directions and topological structures considering the HDP mode, the problem of multi-patch orientations is rarely considered. In fact, the optimization method that forces all substrate domains to adopt a uniform direction is less optimal, because complex principal stress directions are generally involved for topological structures [15]. Therefore, we propose a multi-patch design framework, which divides the substrate domain into several patches and assigns patch-wise uniform path directions, so that co-evolvement of the patch shapes and uni-directions brings up the maximum load-bearing effect. The schematic diagram of our proposed multi-patch printing considering the HDP mode is shown in Fig. 1. After separating the contour offset layer from the substrate based on the improved double smoothing projection (DSP) projection, the material properties in all directions can be simulated through the coordinate transformation of the fundamental orthogonal anisotropic constitutive model [16].

In practical engineering, dynamic issues cannot be overlooked [17–19], especially the research on the printing angle of structures under dynamic loads [20]. Dynamic topology optimization can be divided into two categories [21]: time-domain and frequency-domain. Time-domain optimization focuses on the transient response of the structure [22,23], while frequency-domain optimization emphasizes steady-state vibrations [24,25]. In this paper, we adopt the frequency-

domain method, specifically the common dynamic compliance method [26], to optimize the dynamic response of the structure.

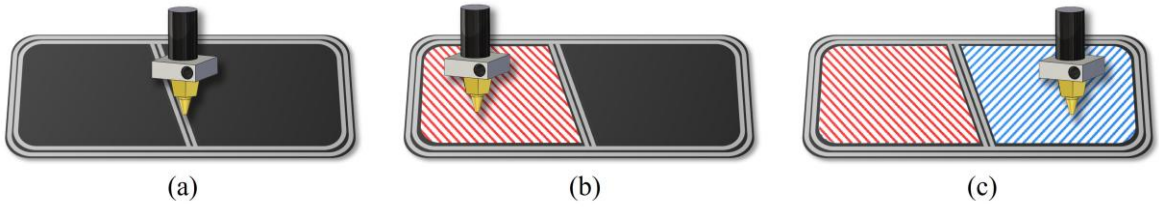

Figure 1: Illustration of the multi-directions HDP pattern (a) Print the boundary layer (b) Print the substrate domain with direction #1 (c) Print the substrate domain with direction #2.

In summary, this study aims at solving the problem of multi-direction & multi-density collaborative optimization considering the patch-wise anisotropic material characteristics under dynamic loads and mixed deposition path pattern. We introduce the improved DSP filter and SOMP (solid orthotropic material with penalty) interpolation method, combined with topological density variables and raster direction variables for concurrent optimization. The extended-SIMP interpolation method is also coupled to divide the patches while evolving their shapes. The main contributions are as follows:

- *Multi-direction & multi-density collaborative optimization method*: A novel multi-direction design framework is proposed to solve the multi-direction-density distribution optimization problem based on dynamic loads and material anisotropy characteristics under HDP mode. Through the improved DSP filtering and SOMP interpolation method, the parallel optimization of topological density and printing direction is achieved.
- *Full-scale material anisotropy modeling and optimization-based dynamic structure generation*: Based on the extended-SIMP method, material properties in different directions are effectively coupled to generate optimal structure and optimal directions of the substrate domain. Precisely separating the contour offset layer and refining the material density distribution in the substrate domain promotes design innovation in terms of efficiency and adaptability in the field of AM.

2 OPTIMIZATION PROBLEM FORMULATION

The time discrete form of the equation of the ndof-freedom discrete structure under simple harmonic load can be expressed as:

$$\mathbf{M}\ddot{\mathbf{u}} + \mathbf{C}\dot{\mathbf{u}} + \mathbf{K}\mathbf{u} = \mathbf{p} \tag{2.1}$$

Where $\mathbf{p}$ represents the time-dependent dynamic load, expressed as $\mathbf{p}(t) = \mathbf{P}e^{i\omega_p t}$, with an amplitude $\mathbf{P}$ and frequency ω_p. $\mathbf{u}$ represents the displacement vector, and its equation can be written as $\mathbf{u}(t) = \mathbf{U}e^{i\omega_p t}$, where $\mathbf{U}$ is the amplitude of the displacement. $\dot{\mathbf{u}}$ and $\ddot{\mathbf{u}}$ represent the first and second order time derivatives of the displacement, i.e., velocity and acceleration, respectively. Therefore, Eqn. (2.1) can be rewritten as:

$$(-i\omega_p^2\mathbf{M} + i\omega_p\mathbf{C} + \mathbf{K})\mathbf{U} = \mathbf{P} \tag{2.2}$$

$$\mathbf{K}_\mathbf{d} = (-i\omega_p^2\mathbf{M} + i\omega_p\mathbf{C} + \mathbf{K}) \tag{2.3}$$

Here $\mathbf{K}_\mathbf{d}$ represents the dynamic stiffness matrix. Since the damping matrix $\mathbf{C}$ is not considered in this paper, the influence of virtual displacement does not need to be considered in the analysis. In

other words, $\mathbf{U}$ is a real number. According to the classical laminate theory, the directional elastic tensor of anisotropic materials can be expressed in the form of Eqn. (2.4) [13,14].

$$\mathbf{D}(\theta) = \mathbf{T}(\theta)\mathbf{D}_0\mathbf{T}(\theta)^T \tag{2.4}$$

Where $\mathbf{D}_0$ is the unrotated elastic tensor and $\mathbf{T}$ is the coordinate transformation matrix; see [13,14] for details. Next, we differentiate the design domain based on the improved DSP method to obtain the substrate domain and boundary layer. The algorithm consists of two main parts, namely, PDE filter and Heaviside projection. First, a PDE filter based on the Helmholtz-type partial differential equation is applied to the initial design variable x :

$$-r^2\nabla^2\tilde{x} + \tilde{x} = x \tag{2.5}$$

Where $\tilde{x}$ is a smoothing variable. r is a length scale parameter, which has a numerical relationship with the classical filter radius R. Then the smoothed variables were truncated using Heaviside projection.

$$\mu = \frac{\tanh(\beta\eta) + \tanh(\beta(\tilde{x} - \eta)}{\tanh(\beta\eta) + \tanh(\beta(1 - \eta)} \tag{2.6}$$

Here β represents the sharpness of the Heaviside function, and the threshold η is 0.95, at which the boundary thickness w can be precisely controlled by the filter radius R [16]:

$$w \approx 0.67R \tag{2.7}$$

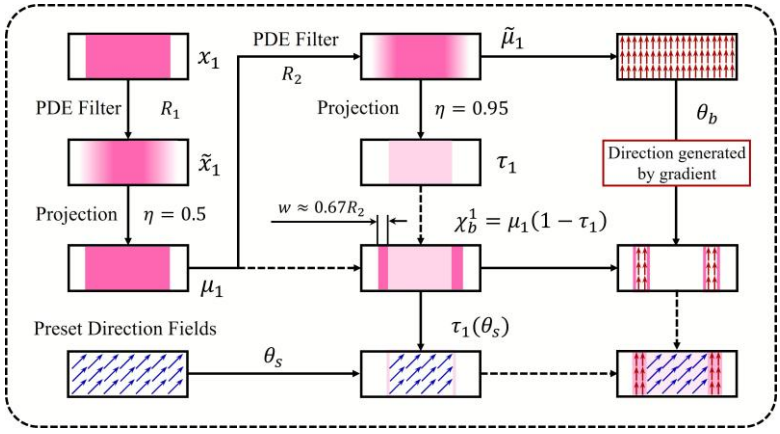

Figure 2: Schematic diagram of the process of dividing the design domain into the substrate domain and the boundary layer through DSP and obtaining the corresponding directions.

Fig. 2 shows a flow chart of separating the substrate domain from the boundary layer when only one substrate domain filling direction is involved. The design variable x_1 is filtered by DSP to obtain the corresponding substrate domain τ_1 and boundary layer χ_b^1. At the same time, we can assign the predefined direction θ_s to the substrate domain τ_1 and obtain the boundary layer direction θ_b through the spatial gradient of the intermediate density field $\tilde{\mu}_1$, through which finally get the distribution of all directions in the design domain. The angle θ_s in Fig. 2 corresponds to $\mathbf{T}\ \theta$ in Eqn. (2.4). This angle is defined by rotating counterclockwise as positive from the x-axis, as shown in Fig. 3. The range of this angle is defined as $\left[-2\pi, 2\pi\right]$.

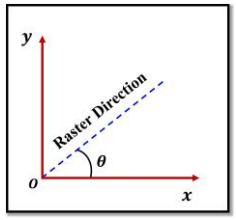

Figure 3: Definition of the direction variable.

Since the directions between the substrate domain and the boundary layer are different, based on the SOMP model the elastic tension and density of the entire structure can be expressed as:

$$D^1(x_1) = D_s\tau_i^p + D_b\mu_1^p(1-\tau_1^p) \tag{2.8}$$

$$\rho^1(x_1) = \rho_s\tau_1 + \rho_b\mu_1(1-\tau_1) \tag{2.9}$$

D_s and D_b in Eqn. (2.8) represent the elastic tension of the substrate domain and boundary layer respectively, which are related to the directions θ_s and θ_b. p represents the penalty factor. Since the printed boundary layer and the substrate are made of the same material, the two densities ρ_s and ρ_b in Eqn. (2.8) are the same and can be uniformly represented by ρ.

Based on the extended-SIMP interpolation, we can treat the substrate domains at different directions as different materials for analysis. When there are N filling directions in the substrate domain, the elastic tension D^N and density interpolation ρ^N of the entire structure can be expressed as follows:

$$D^N(x_1,x_2\ldots x_N) = \sum\nolimits_{i=1}^{N} D_s^i\Xi_i^s + D_b^i\Xi_i^b \tag{2.10}$$

$$\rho^N(x_1,x_2\ldots x_N) = \sum\nolimits_{i=1}^{N} \rho(\psi_i^s + \psi_i^b) \tag{2.11}$$

Here Ξ_i^s, Ξ_i^b, ψ_i^s, ψ_i^b are equations of the design variable $x_i(i=1:N)$, D_s^i and D_b^i represent the elastic tension of the substrate domain and boundary layer corresponding to the i-th direction.

$$\Xi_i^s = (1-\tau_{i-1}^p)(1-\mu_{i-1}^p)\prod\nolimits_{j=i}^{N}\tau_j^p \tag{2.12}$$

$$\Xi_i^b = \sum\nolimits_{i=1}^{N}\left[(1-\tau_i^p)\mu_i^p\prod\nolimits_{j=i+1}^{N}\tau_j^p\right] \tag{2.13}$$

$$\psi_i^s = (1-\tau_{i-1})(1-\mu_{i-1})\prod\nolimits_{j=i}^{N}\tau_j \tag{2.14}$$

$$\psi_i^b = \sum\nolimits_{i=1}^{N}\left[(1-\tau_i)\mu_i\prod\nolimits_{j=i+1}^{N}\tau_j\right] \tag{2.15}$$

We take the case that there are two directions θ_s^1 and θ_s^2 in the substrate domain (N=2) as an example, the structural model is shown in Fig. 4.

It is worth noting that the direction of the boundary layer is calculated based on the gradient. Therefore, its elastic tension is quite different and essentially based on the derivative of the design variable. For example, in this case, there are two boundary layers ψ_1^b and ψ_2^b, and their corresponding directions can be expressed by following equation:

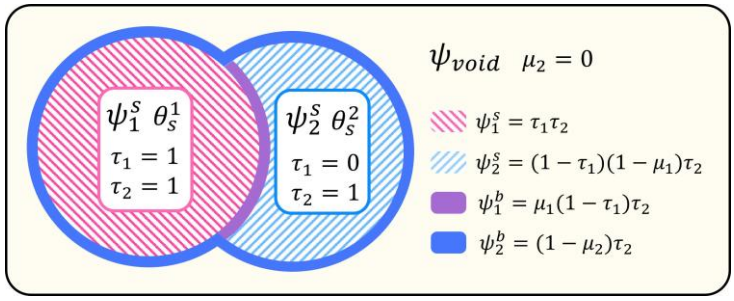

Figure 4: Simple schematic diagram of the substrate domain and boundary layer at multiple directions.

$$\begin{aligned}\theta_b^1 &= \frac{\pi}{2} + \arctan\left(\frac{\partial\tilde{\mu}_1}{\partial y}\Big/\frac{\partial\tilde{\mu}_1}{\partial x}\right)\\ \theta_b^2 &= \frac{\pi}{2} + \arctan\left(\frac{\partial\tilde{\mu}_2}{\partial y}\Big/\frac{\partial\tilde{\mu}_2}{\partial x}\right)\end{aligned} \tag{2.16}$$

Based on all the above preparations, combined with Eqn. (2.1), we take minimizing the overall vibration response under a fixed excitation load as the optimization goal, that is, minimizing the dynamic compliance of the structure [27]. In order to ensure numerical stability, the dynamic compliance norm is defined as the objective function, and the optimization formula is as follows:

$$\begin{aligned}&find: x_i(i=1,\ldots,N), \theta_s^i(i=1,\ldots,N)\\ &\min: Cd = \left\|\mathbf{P}^T\mathbf{U}\right\|\\ &s.t.: \begin{cases}\mathbf{K_d U} = (\mathbf{K} - \omega_p^2\mathbf{M})\mathbf{U} = \mathbf{P}\\ G_i = V_i/\overline{V} - f_i \le 0, (i=1,\ldots,N)\\ x_e \in \left[10^{-3},1\right], \theta_e \in \left[-2\pi, 2\pi\right]\end{cases}\end{aligned} \tag{2.17}$$

In the formula, G_i represents the volume constraint, f_i is the proportion of the substrate domain in each direction, and V_i is the volume calculation formula of the i-th substrate, as shown below:

$$V_i = \sum_{k=1}^{nele}\left[1 - \mu_{i-1}\prod_{j=i}^{N}\mu_j\right] \tag{2.18}$$

Where $nele$ represents the total number of elements corresponding to the finite element mesh.

3 NUMERICAL EXAMPLE

In this section, we will use a half-simply supported beam case to demonstrate the effectiveness of our optimization algorithm. As shown in Fig. 5, in order to better demonstrate the boundary layer effect, a non-design domain is set around its edge. The structure is discretized into 160*160 units, and the material parameters are set as shown in the following table. The load is 200kN with an amplitude $\mathbf{P}$ and a frequency ω_p of 100Hz. The initial directions are set to 0° and 90°, respectively. The volume fraction of two directions is both 0.25. The optimization iteration process is shown in Fig. 6. Combined with Fig. 6, it is not difficult to see that the iteration converges smoothly, and all parameters have been optimized to a certain extent. The dynamic compliance is reduced from 113.25kN·m to 43.85kN·m, and the first eigenfrequency is increased to 967Hz. The two directions finally optimized are 4.21° and 68.23° respectively. In Fig. 7 we also show the directional details of the two substrate domains and the two boundary layers.

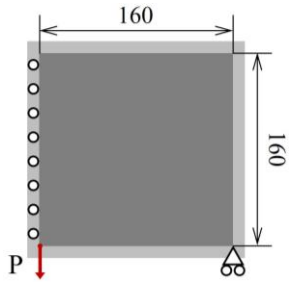

Figure 5: Design domain of simply supported beam.

Material parameters	*Young's modulus in x direction*	*Young's modulus in y direction*	*Poisson's ratio in the xy direction*	*Density*	*Filter radius of density field x_1*	*Filter radius of density field x_2*	*Boundary layer thickness*
Numeric	$E_x = 50\text{GPa}$	$E_y = 25\text{GPa}$	$V_{xy} = 0.4$	$\rho = 1\text{kg}/\text{m}^3$	$R_1 = 6$	$R_2 = 6$	$w = 2$

Table 1: Material parameters used in the optimization.

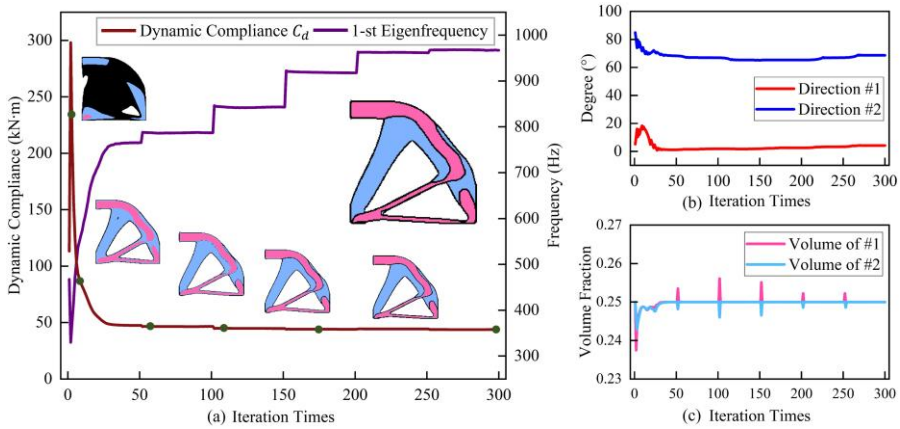

Figure 6: The optimization process: (a) Iterative process of structural dynamic compliance and 1-st eigenfrequency (b) Iterative process of directions of substrate domain (c) Iterative process of volume fraction corresponding to two directions.

The two substrate printing directions are separated by a uniform and clear boundary layer. The clear boundary layer reduces the stress concentration in the transition area of different printing directions, improves the stability of the structure, and ensures that the substrate areas of different printing directions can function independently, avoiding the negative impact of directional mixing on the anisotropy of the material. In addition, the internal angle filling meets the design requirements, indicating that the optimization process fully utilizes the anisotropic properties of the material, aligns the printing direction with the main stress distribution, and thus significantly improves the dynamic performance of the structure.

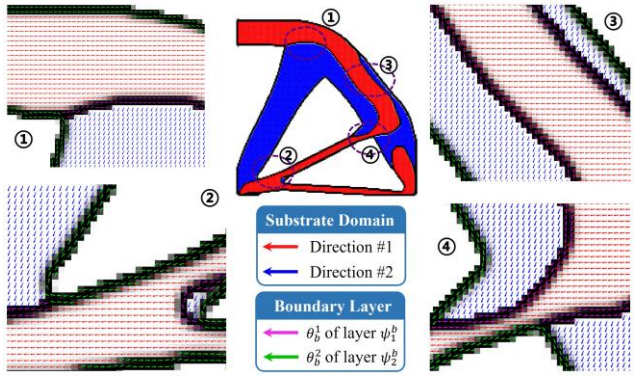

Figure 7: Schematic diagram of printing direction of each area.

In addition, we also explored the impact of different initial substrate domain directions combinations on the optimization results under this design domain, as shown in Fig. 8.

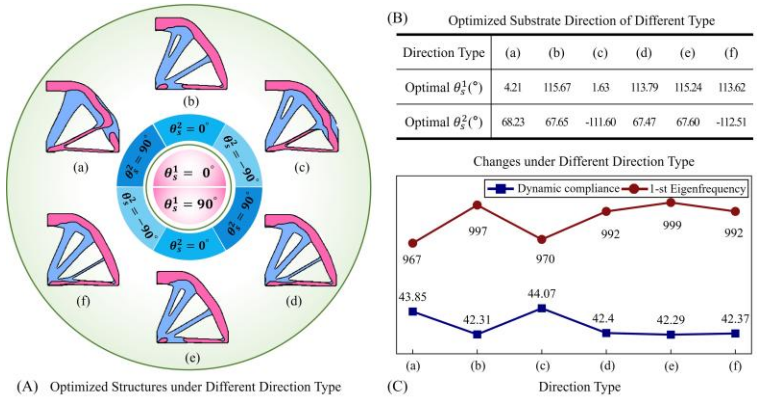

Direction Type	(a)	(b)	(c)	(d)	(e)	(f)
Optimal θ_s^1(°)	4.21	115.67	1.63	113.79	115.24	113.62
Optimal θ_s^2(°)	68.23	67.65	-111.60	67.47	67.60	-112.51

Figure 8: The optimized results under different initial substrate domain directions: (A) The optimized structures under different direction type (B) The optimized substrate direction of different type (C) The dynamic compliance Cd and 1-st eigenfrequency under different direction type.

From Fig. 8(A), we can see that the optimized structures under different initial angle combinations show certain similarities, such as (a) and (c), (b) and (e), and (d) and (f). The directions of the substrate domain obtained by the final optimization also show similar characteristics. For example, the initial angle θ_s^2 of (d) and (f) is symmetrical to each other, and the optimized angles 67.47° and -112.51° are approximately symmetrical about the origin. The similarity of the optimization parameters shown in Fig. 8(B) and (C) stems from the fact that the optimization algorithm naturally converges to directional configurations that balance stress and stiffness when dealing with geometrically symmetric simply supported beam structures and uniform dynamic loads.

The influence of external loads on the optimization results was also investigated. As shown in the Fig. 9, the cantilever beam design domain is discretized into a 200*100 grid, and the filter radius R_1 and R_2 are both set to 8. Material parameters and volume fractions are the same as those of simply supported beam. The amplitude of the excitation was set to 200kN in the downward direction, and the excitation frequency was gradually increased from 100Hz.

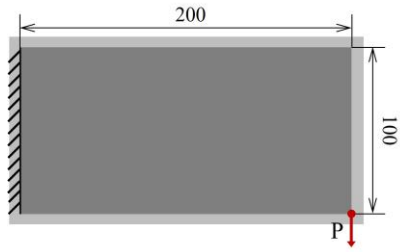

Figure 9: Design domain of cantilever beam.

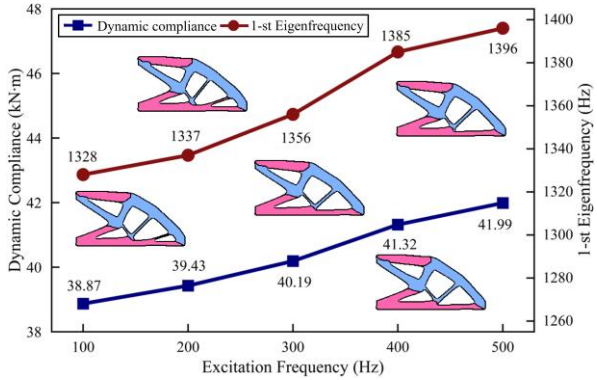

Figure 10: The optimized results under different excitation frequency.

Frequency (Hz)	100	200	300	400	500
Optimal θ_s^1 (°)	1.61	1.78	1.39	1.49	1.39
Optimal θ_s^2 (°)	138.49	139.23	139.20	139.55	138.82

Table 2: Optimization direction under different excitation frequencies.

Combined with Fig. 10 and Table 2, the effect of the excitation frequency on the optimization results is mainly reflected in the dynamic compliance and 1-st eigenfrequency of the structure, while it has little effect on the optimized structural morphology and the two filling angles in the substrate area. This is because the filling angle is mainly determined by the material distribution and anisotropic properties in the topology optimization, rather than being directly driven by the dynamic load. The optimization goal (minimizing dynamic compliance) adjusts the dynamic response of the structure more, while the directional optimization depends on the geometry and material properties of the substrate area.

4 CONCLUSION

This paper proposes a topology optimization method for multi-patch FDM printing, aiming at improving the structural performance under dynamic loads. The material anisotropy is incorporated so that co-optimization of the structural topology and patch-wise printing directions are conducted. We use the improved DSP projection and the SOMP interpolation method to accurately distinguish the contour offset layer and the base area, and use the extended SIMP method to divide the

substrate domains into multiple patches with different printing directions. The superiority of this method is verified by a series of numerical examples.

The results show that multi-patch FDM printing topology optimization has obvious advantages in dealing with dynamic loads, especially in enhancing the dynamic stiffness and stability of the structure. Compared with the traditional single-patch design, the multi-directional design can better utilize the anisotropic properties of the materials, effectively reducing stress concentration and enhancing the structural dynamic stability. In addition, the study found that the choice of printing direction is mainly determined by the topological structure and is less affected by the load size and frequency.

In summary, this study provides important theoretical support and practical solutions for the structural design of multi-patch FDM printing in dynamic environments, providing a foundation for the further development of dynamic structural design for AM.

5 ACKNOWLEGEMENTS

The authors would like to acknowledge the support from Key R&D Program of Rizhao City, China (2021ZDYF010101).

Kaiyuan Meng, https://orcid.org/0009-0007-0845-3388
Jikai Liu, https://orcid.org/0000-0002-9732-3791

REFERENCES

[1] Liu, J.; Ma, Y.: A survey of manufacturing-oriented topology optimization methods, Advances in Engineering Software, 2016, 100, 161–75. https://doi.org/10.1016/j.advengsoft.2016.07.017

[2] Xu, S.; Liu, J.; He, D.; Tang, K.; Yaji, K.: Self-support structure topology optimization for multi-axis additive manufacturing incorporated with curved layer slicing, Computer Methods in Applied Mechanics and Engineering, 2025 438 117841. https://doi.org/10.1016/j.cma.2025.117841

[3] Xu, S.; Liu, J.; Yaji, K.; Lu, L.: Topology optimization for hybrid additive-subtractive manufacturing incorporating dynamic process planning, Computer Methods in Applied Mechanics and Engineering, 2024, 431, 117270. https://doi.org/10.1016/j.cma.2024.117270

[4] Liu, J.; Zhang, C.; Zou, B.; Li, L.; Yu, H.: Topology optimization for vat photopolymerization 3D printing of ceramics with flushing jet accessibility constraint, Virtual and Physical Prototyping, 2024, 19, e2303717. https://doi.org/10.1080/17452759.2024.2303717

[5] Guo, Y.; Liu, J.; Ahmad, R.; Ma, Y.: Concurrent structural topology and fabrication sequence optimization for multi-axis additive manufacturing, Computer Methods in Applied Mechanics and Engineering, 2025, 435, 117627. https://doi.org/10.1016/j.cma.2024.117627

[6] Liu, S.; Li, Q.; Hu, J.; Chen, W.; Zhang, Y.; Luo, Y.; et al.: A Survey of Topology Optimization Methods Considering Manufacturable Structural Feature Constraints for Additive Manufacturing Structures, Additive Manufacturing Frontiers, 2024, 3, 200143. https://doi.org/10.1016/j.amf.2024.200143

[7] Zhang, P.; Liu, J.; To, A. C.: Role of anisotropic properties on topology optimization of additive manufactured load bearing structures, Scripta Materialia, 2017, 135, 148–52. https://doi.org/10.1016/j.scriptamat.2016.10.021

[8] Xia, Q.; Shi, T.: Optimization of composite structures with continuous spatial variation of fiber angle through Shepard interpolation, Composite Structures, 2017, 182, 273–82. https://doi.org/10.1016/j.compstruct.2017.09.052

[9] Lee, J.; Kim, D.; Nomura, T.; Dede, E. M.; Yoo, J.: Topology optimization for continuous and discrete orientation design of functionally graded fiber-reinforced composite structures.

Composite Structures, 2018, 201, 217–33. https://doi.org/10.1016/j.compstruct.2018.06.020
[10] Papapetrou, V. S.; Patel, C.; Tamijani, A. Y.: Stiffness-based optimization framework for the topology and fiber paths of continuous fiber composites, Composites Part B: Engineering, 2020, 183, 107681. https://doi.org/10.1016/j.compositesb.2019.107681
[11] Ren, H.; Wang, D.; Liu, G.; Rosen, D. W.; Xiong, Y.: Concurrent optimization of structural topology and toolpath for additive manufacturing of continuous fiber-reinforced polymer composites, Computer Methods in Applied Mechanics and Engineering, 2024, 430, 117227. https://doi.org/10.1016/j.cma.2024.117227
[12] Liu, J.; Ma, Y.; Qureshi, A. J.; Ahmad, R.: Light-weight shape and topology optimization with hybrid deposition path planning for FDM parts, Int J Adv Manuf Technol, 2018, 97, 1123–35. https://doi.org/10.1007/s00170-018-1955-4
[13] Xu, S.; Huang, J.; Liu, J.; Ma, Y.: Topology Optimization for FDM Parts Considering the Hybrid Deposition Path Pattern, Micromachines, 2020, 11, 709. https://doi.org/10.3390/mi11080709
[14] Meng, K.; Fu, J.; Qu, D.; Li, L.; Liu, J.: Dynamic topology optimization incorporating the material anisotropy feature for 3D printed fiber composite structures, Finite Elements in Analysis and Design, 2025, 243, 104281. https://doi.org/10.1016/j.finel.2024.104281
[15] Jiang, D.; Hoglund, R.; Smith, D. E.: Continuous Fiber Angle Topology Optimization for Polymer Composite Deposition Additive Manufacturing Applications, Fibers, 2019, 7, 14. https://doi.org/10.3390/fib7020014
[16] Luo, Y.; Li, Q.; Liu, S.: Topology optimization of shell–infill structures using an erosion-based interface identification method, Computer Methods in Applied Mechanics and Engineering, 2019, 355, 94–112. https://doi.org/10.1016/j.cma.2019.05.017
[17] Zargham, S.; Ward, T.A.; Ramli, R.; Badruddin, I.A.: Topology optimization: a review for structural designs under vibration problems, Struct Multidisc Optim, 2016, 53,
1157–77. https://doi.org/10.1007/s00158-015-1370-5
[18] Mukherjee, S.; Lu, D.; Raghavan, B.; Breitkopf, P.; Dutta, S.; Xiao, M.; et al.: Accelerating Large-scale Topology Optimization: State-of-the-Art and Challenges, Arch Computat Methods Eng, 2021, 28, 4549–71. https://doi.org/10.1007/s11831-021-09544-3
[19] Li, Q.; Sigmund, O.; Jensen, J.S.; Aage, N.: Reduced-order methods for dynamic problems in topology optimization: A comparative study, Computer Methods in Applied Mechanics and Engineering, 2021, 387, 114149. https://doi.org/10.1016/j.cma.2021.114149
[20] Ding, H.; Xu, B.; Huang, C.; Duan, Z.: A multi-scale discrete material optimization model for optimization of structural topology and material orientations to minimize dynamic compliance, Struct Multidisc Optim, 2021, 64, 1343–65. https://doi.org/10.1007/s00158-021-02922-2
[21] Zhao, J.; Yoon, H.; Youn, B.D.: An efficient concurrent topology optimization approach for frequency response problems. Computer Methods in Applied Mechanics and Engineering 2019;347:700–34. https://doi.org/10.1016/j.cma.2019.01.004
[22] Jiang, X.; Zhang, W.; Teng, X.; Chen, X.: Concurrent Topology Optimization of Multi-Scale Composite Structures Subjected to Dynamic Loads in the Time Domain, Mathematics 2023, 11, 3488. https://doi.org/10.3390/math11163488
[23] Zhang, X.; Kang, Z.: Dynamic topology optimization of piezoelectric structures with active control for reducing transient response, Computer Methods in Applied Mechanics and Engineering, 2014, 281, 200–19. https://doi.org/10.1016/j.cma.2014.08.011
[24] Meng, F.; Meng, L.; Wang, J.; Zhu, J.; Wang, B.P.; Yuan, S.; et al.: Topology optimization for minimum dynamic compliance using an antiresonant frequency constraint, Structural and Multidisciplinary Optimization, 2024, 67, 1–19. https://doi.org/10.1007/s00158-024-03878-9
[25] Zhao, J.; Yoon, H.; Youn, B.D.: Concurrent topology optimization with uniform microstructure for minimizing dynamic response in the time domain, Computers & Structures, 2019, 22, 98–117. https://doi.org/10.1016/j.compstruc.2019.07.008

[26] Niu, B.; He, X.; Shan, Y.; Yang, R.: On objective functions of minimizing the vibration response of continuum structures subjected to external harmonic excitation, Struct Multidisc Optim, 2018, 57, 2291–307. https://doi.org/10.1007/s00158-017-1859-1
[27] Du, J.; Olhoff, N.: Minimization of sound radiation from vibrating bi-material structures using topology optimization, Struct Multidisc Optim, 2007, 33:, 05–21. https://doi.org/10.1007/s00158-006-0088-9